

An Approximate Approach to Determining the Permittivity and Permeability near $\lambda/2$ Resonances in Transmission/Reflection Measurements

Sung Kim* and James Baker-Jarvis

Abstract—We present a simple and straightforward approximate approach to removing resonant artifacts that arise in the material parameters extracted near half-wavelength resonances that arise from transmission/reflection (T/R) measurements on low-loss materials. In order to determine material parameters near one such $\lambda/2$ resonance, by means of the 1st-order regressions for the input impedance of the sample-loaded transmission line, we approximate the characteristic impedance of the sample-filled section that is, in turn, dependent either on the relative wave impedance in a coaxial transmission line or on the relative permeability in a rectangular waveguide case. The other material parameters are then found, supplemented with the refractive index obtained from the conventional T/R method. This method applies to both coaxial transmission line and rectangular waveguide measurements. Our approach is validated by use of S -parameters simulated for a low-loss magnetic material, and is also applied to determine the relative permittivity and permeability from S -parameters measured for nylon and lithium-ferrite samples. The results are discussed as compared to those from the well-known Nicolson-Ross-Weir (NRW) method and are experimentally compared to those from the Baker-Jarvis (BJ) method as well.

1. INTRODUCTION

Precise knowledge of electric permittivities, magnetic permeabilities, and electric and magnetic losses of materials is a fundamental requisite for scientific research on materials and provides such data for the engineering applications of these materials. Depending on forms of test material samples and classes of measurement data of interest, numerous measurement techniques and algorithms for material characterizations have been proposed, and various methods are extensively summarized in [1–4].

Solids are the major class of materials that are measured over broad frequency ranges. Because broadband transmission and reflection coefficients are measurable by employing transmission-line-type sample fixtures, transmission/reflection (T/R) methods have been widely adopted for broadband measurements on solid material samples. Existing T/R methods for extracting material parameters, whether those algorithms are reformulated or not, have been unable to resolve two major inherent issues. The inherent weaknesses in current algorithms show up with dispersive or low-loss materials. First, explicit (non-iterative) T/R methods involve a procedure for calculating a natural logarithm containing measured transmission/reflection data, and the branch cut when the material being tested is dispersive is ambiguous. The other issue stems from standing waves occurring within a low-loss sample due to the impedance mismatch to air of the transmission line on both sides of the sample faces where the dimension is an integer multiple of a half wavelength. Such a geometrical resonance is

Received 13 December 2013, Accepted 26 January 2014, Scheduled 30 January 2014

* Corresponding author: Sung Kim (sung.x.kim@nist.gov).

The authors are with the Electromagnetics Division, National Institute of Standards and Technology, 325 Broadway, Boulder, CO 80305, USA.

occasionally called ‘Fabry-Perot’ resonances in the literature [5–7]. Half-wavelength ($\lambda/2$) resonances in the transmission and reflection coefficients, measured for low-loss samples, make the extracted permittivities and permeabilities oscillatory, and give rise to considerable degradation of accuracy of the material characterizations, with those resonant artifacts.

This resonance issue has been long recognized, and several efforts have been made to address it [5, 8–10]. All of these proposed methods, however, can only remove the artifacts for permittivities extracted with T/R methods at the $\lambda/2$ resonances. For the $\mu_r = 1$ assumption for low-loss dielectric materials, Boughriet et al. [8] reformulated the Nicolson-Ross-Weir (NRW) method [11, 12] smoothing out permittivity data at the resonances. Assuming that the phase uncertainties of the reflection measurements are dominant at the resonances, Hasar [9, 10] derived an amplitude-only method for determining permittivities of low-loss dielectric materials. Chalapat et al. [5] proposed incorporating a reference-plane-invariant method as modified from the Baker-Jarvis (BJ) technique [13, 14] into a non-iterative method derived similarly from the NRW algorithm that uses the group-delay measurement data, and successfully reduced uncertainties for the calculated permittivities, compared to conventional T/R methods. While all of these approaches are inventive, they remain limited to fixing artifacts for only dielectric material measurements.

In this paper, we present a methodology for determining both permittivities and permeabilities of low-loss materials around the half-wavelength resonances. In the following, we first delineate the $\lambda/2$ resonance issue for the conventional T/R method. Along with an intuitive explanation about the input impedance behavior for a sample-loaded transmission line at the resonance, we provide a starting point for the method we have developed. With an assumption that the material sample treated in this work is non-dispersive, the 1st-order regression coefficients for the input impedance are used to calculate the characteristic impedance of the sample-filled section that is a function of the wave impedance of the material filling a coaxial transmission line or is a function of the permeability filling a rectangular waveguide. To this end, the other material parameters are calculated with help of the refractive index obtained from the conventional T/R method. The only assumption made in this paper is that the characteristic impedance of the material-filled section of the transmission line has a flat response at the frequencies near the half-wavelength resonance. This approach can be applied to simultaneously characterize both permittivity and permeability data of any low-loss, non-dispersive materials.

2. THEORY

2.1. The Issue for Conventional T/R Methods

To begin with, let us review the issue that arises in conventional T/R methods, often referred to as the Nicolson-Ross-Weir (NRW) method [11, 12], Baker-Jarvis (BJ) iterative method [13, 14], etc.. These T/R methods determine the complex permittivity and permeability of a material sample placed in a transmission line from the measured total reflection and transmission coefficients (S -parameters) of the transmission line. Fig. 1 shows the schematic of the measurement on S -parameters (together with input impedance (Z_{in}) to be used in Sections 2.2 and 2.3 to develop our new approximate approach) for the transmission line loaded with a test material whose refractive index, relative wave impedance, absolute permittivity, absolute permeability, propagation constant, and characteristic impedance are denoted as n , ς , ε , μ , γ , and Z , respectively. In Fig. 1, the parameters with the subscript 0 mean the ones for the air-filled sections, except that ς_0 is the absolute value (not the relative value as ς), which is 377Ω . The S -parameters measured to implement the NRW method that requires reference planes 1 and 2 at the sample faces in Fig. 1 are represented by

$$S_{11} = S_{22} = \frac{\Gamma(1-t^2)}{1-\Gamma^2 t^2}, \quad (1)$$

$$S_{21} = S_{12} = \frac{t(1-\Gamma^2)}{1-\Gamma^2 t^2}, \quad (2)$$

where t is the propagation factor and Γ is the reflection coefficient of the interface. These relate the material parameters via

$$t = \exp(-\gamma L) \quad (3)$$

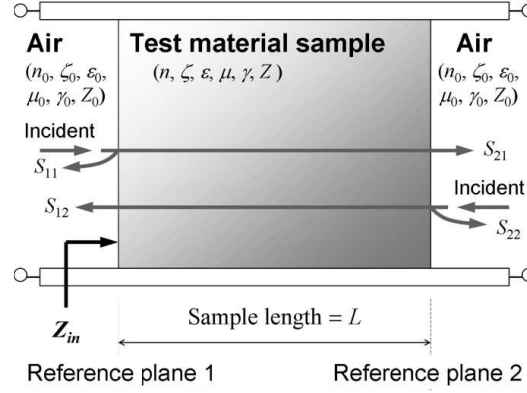


Figure 1. Schematic of the S -parameter and input impedance measurement of the sample-loaded transmission line.

and

$$\Gamma = \frac{\frac{\mu}{\gamma} - \frac{\mu_0}{\gamma_0}}{\frac{\mu}{\gamma} + \frac{\mu_0}{\gamma_0}}, \quad (4)$$

where L is the sample length. In Eqs. (3) and (4), the propagation constant γ is given by

$$\gamma = j \sqrt{\frac{\omega^2 \epsilon_r \mu_r}{c^2} - \left(\frac{2\pi}{\lambda_c}\right)^2}, \quad (5)$$

where j is the imaginary unit defined as $j = \sqrt{-1}$, and ϵ_r and μ_r are the relative permittivity and permeability of the sample. c is the speed of light, ω the angular frequency, and λ_c the cutoff wavelength of the rectangular waveguide (λ_c is infinite for a coaxial transmission line). We see that we can determine the permittivity and permeability from measured S -parameters by solving Eqs. (1) and (2) for ϵ_r and μ_r .

Instead of inserting Eqs. (3) and (4) into Eqs. (1) and (2), the NRW technique involves explicit computations of Γ and t with measured S_{11} and S_{21} , such as

$$\Gamma = X \pm \sqrt{X^2 - 1}, \quad (6)$$

with

$$X = \frac{(S_{11}^2 - S_{21}^2) + 1}{2S_{11}}, \quad (7)$$

and

$$t = \frac{(S_{11} + S_{21}) - \Gamma}{1 - (S_{11} + S_{21})\Gamma}, \quad (8)$$

and then analytically finding the relative permeability and permittivity with Eqs. (6), (7) and (8), where

$$\mu_r = \frac{1 + \Gamma}{(1 - \Gamma) \Lambda \sqrt{(1/\lambda_0^2) - (1/\lambda_c^2)}} \quad (9)$$

and

$$\epsilon_r = \frac{\lambda_0^2}{\mu_r} \left(\frac{1}{\Lambda^2} + \frac{1}{\lambda_c^2} \right), \quad (10)$$

where λ_0 is the free-space wavelength. In Eqs. (9) and (10), Λ is the guided wavelength that has appeared in the literature [12] as

$$\frac{1}{\Lambda^2} = - \left[\frac{1}{2\pi L} \ln \left(\frac{1}{t} \right) \right]^2. \quad (11)$$

The sign in Eq. (6) should be chosen so that $|\Gamma| \leq 1$ because the sample under test is passive. If the sample length exceeds a half wavelength, the logarithm in Eq. (11) can be multivalued. If the measured group delay is smooth enough at measurement frequencies, we can use this to select the correct branch of the logarithm [12]. If the material sample possesses a dispersive characteristic, the correct branch cut will remain ambiguous. However, this branch-cut ambiguity is out of the scope of this paper, and non-dispersive materials are assumed throughout this work.

In contrast to the NRW method employing Eqs. (9) and (10), the BJ method iteratively solves the following equations as reformulated from Eqs. (1) and (2) for ε_r and μ_r :

$$S_{11}S_{22} - S_{21}S_{12} = \exp[-2\gamma_0(L_{air} - L)] \frac{\Gamma^2 - t^2}{1 - \Gamma^2 t^2}, \quad (12)$$

$$\frac{S_{21} + S_{12}}{2} = \exp[-\gamma_0(L_{air} - L)] \frac{t(1 - \Gamma^2)}{1 - \Gamma^2 t^2}, \quad (13)$$

where L_{air} represents the entire length of the sample-fixtured transmission line, and $L_{air} \geq L$. For the BJ iteration method, the reference planes for the S -parameter measurement are not necessarily at the front and back faces of the sample as in the NRW method. The determinant (12) of the scattering matrix and arithmetic mean (13) of the transmission coefficients are functions of $L_{air} - L$, not merely of L . Therefore, the BJ iteration method is called the reference-plane invariant.

Taking the TEM case for simplicity, we rewrite the equations in a different way to clarify the significant inherent issue of the conventional T/R methods. From Eq. (10) with $\lambda_c = \infty$ and Eq. (11), we obtain the refractive index n of the test material as

$$n = n' - jn'' = \pm \sqrt{\varepsilon_r \mu_r} = \pm j \frac{\lambda_0}{2\pi L} \ln \left(\frac{1}{t} \right). \quad (14)$$

From Eqs. (6) and (7), we have

$$\Gamma^2 - \Gamma \left[\frac{1 - (S_{21}^2 - S_{11}^2)}{S_{11}} \right] + 1 = 0. \quad (15)$$

The substitution of the relation of Γ to the relative wave impedance ς , $\Gamma = (\varsigma - 1)/(\varsigma + 1)$, into Eq. (15) leads to the expression of ς as a function of measured S_{11} and S_{21} :

$$\varsigma = \varsigma' + j\varsigma'' = \pm \sqrt{\frac{\mu_r}{\varepsilon_r}} = \pm \sqrt{\frac{(1 + S_{11})^2 - S_{21}^2}{(1 - S_{11})^2 - S_{21}^2}}. \quad (16)$$

The signs in Eqs. (14) and (16) should be chosen so that $n'' \geq 0$ and $\varsigma' \geq 0$, taking passivity constraints into account. The relative permittivity and permeability can be respectively found from $\varepsilon_r (= \varepsilon'_r - j\varepsilon''_r) = n/\varsigma$ and $\mu_r (= \mu'_r - j\mu''_r) = n \cdot \varsigma$ with n and ς from Eqs. (14) and (16). Note that Eq. (16) has been adopted in the literature to extract negative permittivities and/or permeabilities for metamaterials in the TEM case [15, 16].

Equation (16) provides a very convenient way to show how accuracy is lost around half-wavelength resonant frequencies. As a specific example, we use Eqs. (14) and (16) to extract the refractive index, wave impedance, permittivity, and permeability from the measured S -parameters for a nylon sample ($\varepsilon_r \approx 3$) of $L = 15.10$ mm, measured with a coaxial transmission line having inner and outer radii, $a = 1.52$ mm and $b = 3.50$ mm, respectively. The results are shown in Fig. 2. Figs. 2(a) and (b) show S_{11} and S_{21} as measured with Agilent[†] 8510C vector network analyzer (VNA), and we see from the plots that $|S_{11}|$ and $|S_{21}|$ attain their negative and positive peaks at 5.75 GHz, where the length L becomes a half wavelength. We can confirm from Figs. 2(c) and (d) that the refractive index is relatively smooth in the entire measurement frequency range, whereas the wave impedance exhibits a strong resonance at that frequency. In [17], the authors specified that this resonance was due to the fact that Eq. (16) becomes ill-conditioned with $|S_{11}| \approx 0$ and $|S_{21}| \approx 1$ at the half-wavelength resonance for a very low-loss material, and from Eq. (16) ς behaves divergent as a result.

[†] Reference to specific hardware in this article is provided for informational purposes only and constitutes no endorsement by the National Institute of Standards and Technology.

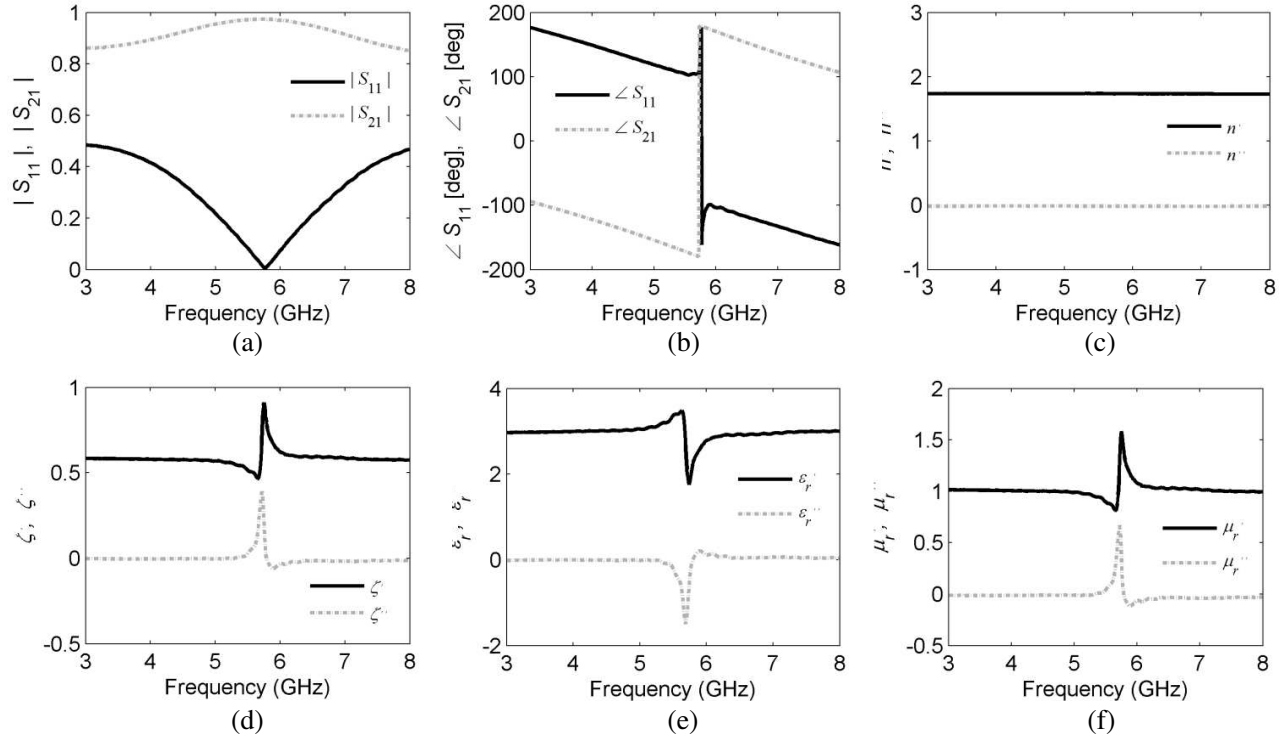


Figure 2. Measured S -parameters and extracted material parameters for nylon ($\epsilon_r \approx 3$) with $L = 15.10$ mm. (a) $|S_{11}|$, $|S_{21}|$, (b) $\angle S_{11}$, $\angle S_{21}$, (c) n' , n'' , (d) ζ' , ζ'' , (e) ϵ_r' , ϵ_r'' , (f) μ_r' and μ_r'' .

The explicit NRW equations generate similar resonances in the extracted permittivity and permeability at the frequency for a half wavelength, because as an intermediate step the algorithm uses Eqs. (6) and (7) to calculate Γ that becomes divergent if $|S_{11}| \approx 0$. With respect to the BJ iteration method based on Eqs. (12) and (13), we observe that the left-hand sides of Eqs. (12) and (13) iterate to nearly the same values, i.e., $|S_{11}S_{22} - S_{21}S_{12}| \approx |S_{21} + S_{12}|/2 \approx 1$, with $|S_{11}|$, $|S_{22}| \approx 0$ and $|S_{21}|$, $|S_{12}| \approx 1$, and thus the material parameters calculated from these equations generate similar artifacts when simultaneously measuring both ϵ_r and μ_r of a low-loss magnetic material. However, note that the BJ method does not have the resonant issue if the method uses only Eq. (13) as a function of S_{21} and S_{12} , not of S_{11} or S_{22} (transmission (T) method), assuming that $\mu_r = 1$ when measuring a dielectric-only material.

In Fig. 2(d), ζ begins to oscillate around 5.3 GHz where $|S_{11}|$ is 0.139, not very small, and S_{21} is not very close to unity ($|S_{21}| \approx 0.966$). All VNAs have a noise floor that is a bottom limit for S -parameters. From a thru measurement under the condition of 10 dBm source power and 128 averaging, the reflection noise floor level of our VNA was read to be about -75 dB, but as the measurement data approach the noise floor, the data may not be sufficiently accurate. This indicates that the oscillation of ζ comes not only from small values but also from this measurement limitation.

In Figs. 2(e) and (f), we see that the extracted permittivity and permeability have resonances similar to the wave impedance but are out of phase relative to one another (ϵ_r goes up and down, while μ_r goes down and up as the frequency is increased around the resonance). This phase relationship results from the fact that the wave impedance has a resonant peak, while the refractive index does not, and consequently, $\epsilon_r = n/\zeta$ and $\mu_r = n \cdot \zeta$ yield these artifacts around the resonance. Actually, both of the NRW and BJ methods as starting at Eqs. (1) and (2) bring about nearly the same n' , n'' , ζ' , ζ'' , ϵ_r' , ϵ_r'' , μ_r' , and μ_r'' , as shown in Fig. 2. To reiterate, the BJ method would not have resonant artifacts when using Eq. (13) to extract only relative permittivity.

Having said that S_{11} should not be too small, we will take the power-series expansion of Eq. (16) to remove the instability under the condition that $|S_{11}| \approx 0$, assuming that S_{11} is very small with respect

to unity, to have good convergence:

$$\zeta \approx 1 - \frac{2}{S_{21}^2 - 1} S_{11} + \frac{2}{(S_{21}^2 - 1)^2} S_{11}^2 - \frac{2(1 + S_{21}^2)}{(S_{21}^2 - 1)^3} S_{11}^3 + \frac{2(1 + 2S_{21}^2)}{(S_{21}^2 - 1)^4} S_{11}^4 + O(S_{11}^5). \quad (17)$$

Note that Eq. (17) can be ill-conditioned with $|S_{21}| \approx 1$ like Eq. (16). Fig. 3 shows the wave impedance calculated from Eqs. (16) and (17) from S -parameters for the nylon sample, taking the terms for the expansion from 1st order to 4th order. We observe in Fig. 3 that the wave impedance from Eq. (17) approaches the result from Eq. (16), with higher order terms included. Similar to that from Eq. (16), ζ from Eq. (17) begins to show the resonant behavior (deviation) around 5.3 GHz, although S_{11} does not appear in its denominators in Eq. (17). We also see that $|S_{21}|$ can be read from Fig. 2(a) to be 0.974 at 5.75 GHz, which is not very close to unity at the resonant frequency. Besides, we observe in Fig. 2(b) that $\angle S_{11} = 110^\circ$ and $\angle S_{21} = -165^\circ$ at 5.3 GHz, whereas $\angle S_{11} = -104^\circ$ and $\angle S_{21} = 170^\circ$ at 6 GHz, and that these S -parameter phases rapidly change around the resonance. Therefore, we can again confirm that measured S_{11} is not accurate enough because of the limitation of the measurement equipment around the $\lambda/2$ resonance. We reiterate that this resonant issue is attributed not only to $|S_{11}| \approx 0$ and $|S_{21}| \approx 1$ but also to measurement limitations.

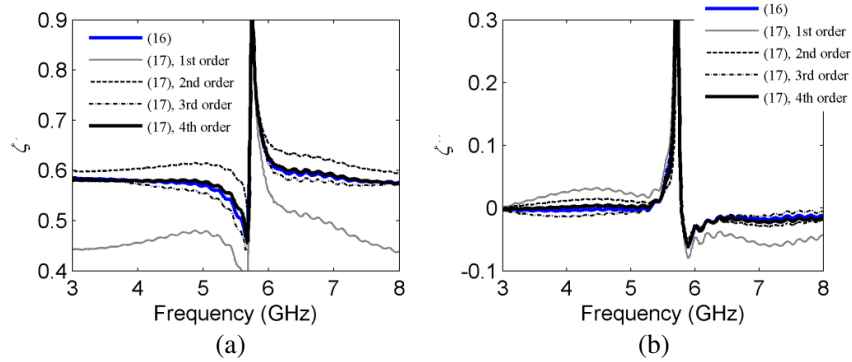


Figure 3. Wave impedance calculated from (16) and (17). (a) ζ' and (b) ζ'' .

We see that any T/R methods derived from Eqs. (1) and (2) suffer from the permittivities and permeabilities contaminated with the artifacts of the wave impedances around $\lambda/2$ resonances. This interpretation can adequately explain the inevitable issue that any conventional T/R methods share, and we can understand that it is very difficult to achieve very clean point-by-point (frequency-by-frequency) material parameters of low-loss materials at each of the measurement frequencies around $\lambda/2$ resonances by use of the conventional T/R methods. A key to removing the artifacts from the material parameters extracted in the T/R measurements will be to derive a reasonable ‘wave impedance’ (‘permeability’ when a rectangular waveguide is used) around the $\lambda/2$ resonance. Section 2.3 will describe our attempt to get rid of the artifact of the wave impedance (or permeability) near the resonance.

2.2. Input Impedance of a Sample-loaded Transmission Line

In this section, we investigate the input impedance of the transmission line as a function of the refractive index and wave impedance of the test material sample installed in the transmission line. Again, consider the transmission line loaded with the material with n and ζ (see Fig. 1). We assume in Fig. 1 that reference plane 1 coincides with the front face of the sample, but the relation of reference plane 2 to the back face of the sample is arbitrary, and that the sample-loaded transmission line is introduced between transmission lines with the characteristic impedance Z_0 that connect to the VNA. In Fig. 1, the input impedance Z_{in} looking from reference plane 1 is represented by

$$Z_{in} = R + jX = Z \frac{Z_0 + Z \tanh(\gamma L)}{Z + Z_0 \tanh(\gamma L)}, \quad (18)$$

where R and X are respectively the real (resistive) and imaginary (reactive) parts of the input impedance of the loaded transmission line. In Eq. (18), the propagation constant and characteristic impedance of the sample-filled section are given by

$$\begin{aligned} \gamma &= jk_0n \quad (\text{coaxial transmission line}) \\ &= j\sqrt{(k_0n)^2 - \left(\frac{2\pi}{\lambda_c}\right)^2} \quad (\text{rectangular waveguide}) \end{aligned} \tag{19}$$

and

$$\begin{aligned} Z &= Z' + jZ'' \\ &= \frac{\zeta\zeta_0}{2\pi} \ln\left(\frac{b}{a}\right) \quad (\text{coaxial transmission line}) \\ &= \frac{j\omega\mu_r\mu_0}{\gamma} = \frac{\omega\mu_r\mu_0}{\sqrt{(k_0n)^2 - (2\pi/\lambda_c)^2}}, \quad (\text{rectangular waveguide}) \end{aligned} \tag{20}$$

where k_0 and ζ_0 are the wavenumber and absolute wave impedance (377Ω) in air, and a and b are the radii of the inner and outer conductors of the coaxial transmission line.

Figure 4 shows the real and imaginary parts R and X of the input impedance Z_{in} calculated from Eq. (18) with $Z_0 = 50 \Omega$ and $L = 20 \text{ mm}$, $a = 1.52 \text{ mm}$, and $b = 3.50 \text{ mm}$ for the sample-loaded coaxial transmission line. Here, it is assumed that the sample is such a low-loss material that the imaginary parts n'' and ζ'' are negligible, and n and ζ are simply real values. For plotting R and X in Figs. 4(a) and (b), n is varied with ζ fixed at 0.4, whereas for the plots in Figs. 4(c) and (d) ζ is varied with n set at 1.0. We observe from the latter two plots that, if $\zeta \neq 1.0$, the $\lambda/2$ resonance occurs at the frequency for $R = Z_0 (= 50)$, and $X = 0$. Fig. 4 shows how varying n shifts the curves of both R and X along the frequency axis, and also that changing ζ brings about different shapes of R and X curves

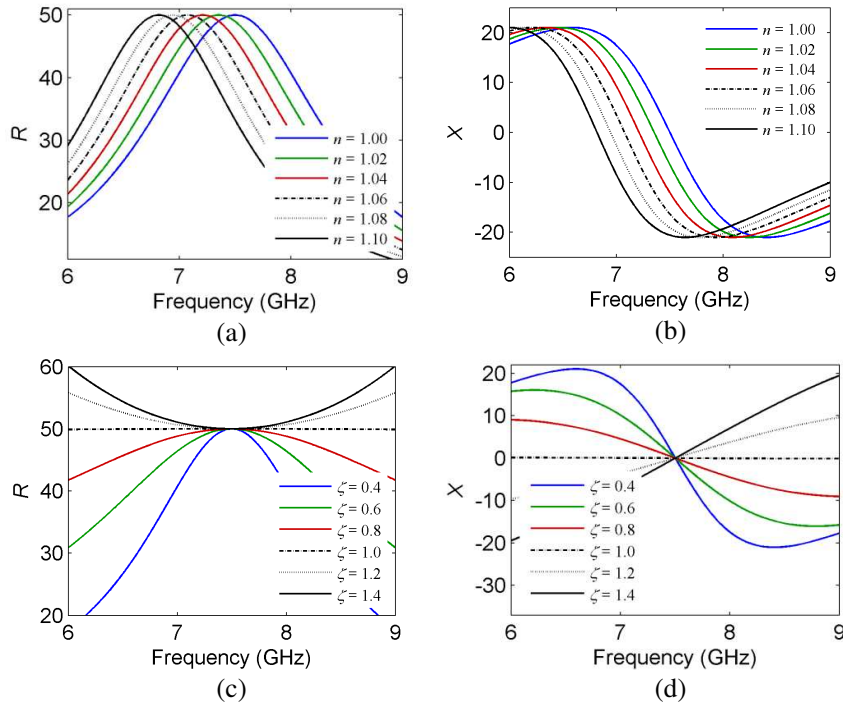


Figure 4. Real and imaginary parts R and X of the input impedance Z_{in} of the transmission line loaded with the sample of n and ζ calculated from (18). (a) R with n varied and $\zeta = 0.4$, (b) X with n varied and $\zeta = 0.4$, (c) R with $n = 1.0$ and ζ varied, and (d) X with $n = 1.0$ and ζ varied.

that retain the same frequency of intersection $R = Z_0$ and $X = 0$. This means that n determines the resonant frequency and ς plays a main role in the gradient changes of R and X . Therefore, we will be able to inversely calculate n from the measured resonant frequency and ς from the gradients of the measured input impedance in R and X . Note that Fig. 4(c) demonstrates that $\varsigma < 1$ and $\varsigma > 1$ give respectively maximal and minimal values to R at the resonant frequency. In other words, the half-wavelength resonant transmission line with $\varepsilon_r > \mu_r$ can be represented by a parallel lumped-element resonant circuit and that with $\varepsilon_r < \mu_r$ is equivalent to a series resonant circuit [18, 19].

2.3. Approximate Approach to the Characteristic Impedance Determination near the $\lambda/2$ Resonance

We approximate the gradients of the real and imaginary parts R and X of the measured input impedance Z_{in} in order to calculate the characteristic impedance Z of the sample-filled section, assuming that Z is constant around the $\lambda/2$ resonant frequency. Fig. 5 illustrates some 1st-order regressions for fitting the real and imaginary parts R and X of the input impedance Z_{in} of the sample-loaded transmission line. In Figs. 5(a) and (b), the resonant frequency band is divided into two regions, I: $f_A - f_0$ and II: $f_0 - f_B$, denoting f_0 as the center frequency and f_A and f_B as the start and stop frequencies at the resonance. f_0 is chosen so that R is the maximal or minimal at that frequency and X is equal to zero at the same time. In these frequency regions, the regression lines for approximating measured R and X are expressed with the 1st order: $R = a_1 f + a_2$ and $X = b_1 f + b_2$ in region I, and $R = c_1 f + c_2$ and $X = d_1 f + d_2$ in region II. The regression coefficients, a_1 , b_1 , c_1 , and d_1 , can be represented as

$$a_1 = \frac{R(f_0) - R(f_A)}{f_0 - f_A}, \quad (21)$$

$$b_1 = \frac{X(f_0) - X(f_A)}{f_0 - f_A}, \quad (22)$$

$$c_1 = \frac{R(f_B) - R(f_0)}{f_B - f_0}, \quad (23)$$

$$d_1 = \frac{X(f_B) - X(f_0)}{f_B - f_0}, \quad (24)$$

where R and X are given by Eq. (18) with Eqs. (19) and (20) that are functions of n and ς for the coaxial transmission line (μ_r for the rectangular waveguide, instead of ς). Here, n is acquired from the conventional T/R method and is substituted into the equations. We can readily solve Eqs. (21) and (22) for the transmission-line characteristic impedance Z in region I, and Eqs. (23) and (24) for the one in region II. Note that if the frequencies f_0 , f_A , and f_B are very high, a_1 , b_1 , c_1 , and d_1 may be very small, resulting in degraded accuracy for Z . Therefore, we use the values in GHz for f_0 , f_A , and f_B when the measurement frequency is in the GHz range. In this paper, we employ the Newton-Raphson method to iteratively solve Eqs. (21)–(24) with the proper initial values chosen from outside the resonance.

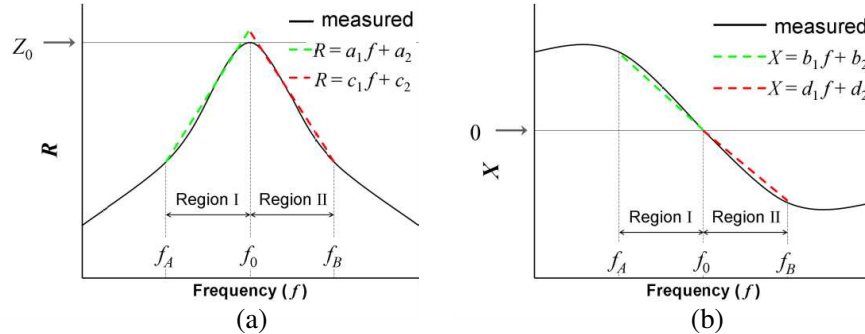


Figure 5. Illustration of the regressions for the real and imaginary parts R and X of the input impedance Z_{in} . (a) R and (b) X .

In the case when a coaxial transmission line is used, we can find the wave impedance with a knowledge of $Z(= Z' + jZ'')$:

$$\zeta = \frac{2\pi Z}{\epsilon_0 \ln\left(\frac{b}{a}\right)}. \tag{25}$$

The relative permittivity and permeability can be obtained with ζ from Eq. (25) and n from Eq. (14); i.e., $\epsilon_r = n/\zeta$ and $\mu_r = n \cdot \zeta$.

If the transmission line is a rectangular waveguide, the relative permeability can be calculated with known Z as follows:

$$\mu_r = \frac{\gamma Z}{j\omega\mu_0} = \frac{\sqrt{(k_0 n)^2 - (2\pi/\lambda_c)^2}}{\omega\mu_0} Z. \tag{26}$$

The permittivity can then be calculated from $\epsilon_r = n^2/\mu_r$ with μ_r from Eq. (26) and n from Eq. (10) along with Eq. (11) ($n = \pm\sqrt{\epsilon_r\mu_r} = \pm\lambda_0\sqrt{1/\Lambda^2 + 1/\lambda_c^2}$). Note that for our approximation to work, we must assume that the sample has non-dispersive material parameters around the resonance so that we are allowed to get flat Z from the approximation near the resonant frequency. This assumption simultaneously guarantees that we do not suffer from the branch cut ambiguity when we calculate n from Eq. (14) (or Eq. (10) with Eq. (11)). To clarify the order of computing the parameters at each step for obtaining the permittivity and permeability, the flow diagram in Fig. 6 summarizes the computation procedure, depending on whether we use a coaxial transmission line or rectangular waveguide. Fig. 6 shows that once measuring the S -parameters and input impedance Z_{in} (convertible from the S -parameters) for the sample, the refractive index n is first acquired in the same manner as the ordinary T/R method, and the regression coefficients $a_1, b_1, c_1,$ and d_1 are calculated from Z_{in} to get the characteristic impedance Z of the loaded section. A sequence of these computations does not involve any complicated tasks. Also, note in Fig. 6 that the only difference between the coaxial transmission line and rectangular waveguide measurements is that in the coaxial line case the wave impedance ζ is

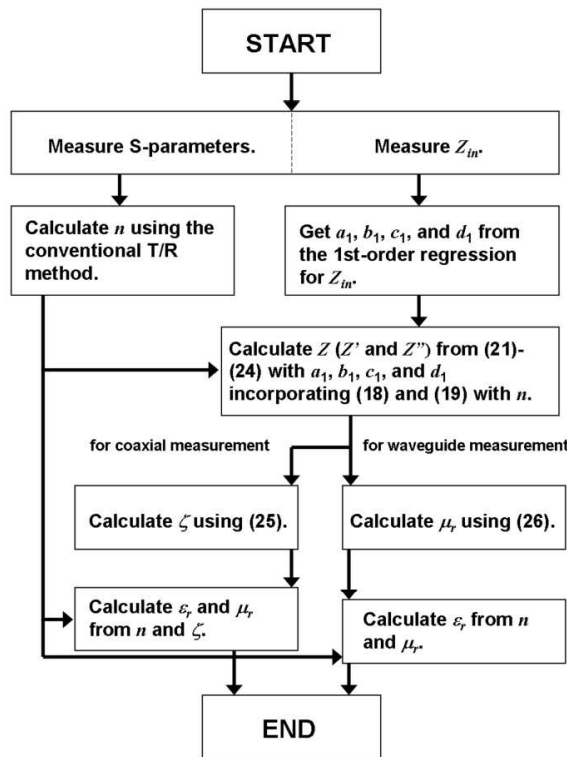


Figure 6. Flow diagram for the computation procedure.

calculated from Z while the relative permeability μ_r is immediately found in the rectangular waveguide case, and that the other material parameters then follow and are easily found in both cases.

Essentially, the conventional T/R methods require at least two equations (S_{11} and S_{21}) (the BJ method makes full use of S -parameters, S_{11} , S_{22} , S_{21} , and S_{12}) to solve two unknowns (permittivity and permeability). In the early stage of this work, we tried using Eq. (2) for measured S_{21} and Eq. (18) for measured input impedance Z_{in} instead of immediate use of Eq. (1) for S_{11} . However, we got almost the same ζ as that from the conventional T/R methods. Moreover, instead of Eq. (1), we attempted to use equations for the resonant frequency f_0 and quality (Q) factor at a $\lambda/2$ resonance, but we observed that measured Q of various material samples appeared to be too low (e.g., $Q = 1$ to 3 for a nylon sample) to obtain sufficiently accurate ε_r and μ_r from f_0 and Q measurements.

3. RESULTS AND DISCUSSION

In order to validate our approximate technique, we employed S -parameters obtained with the full-wave simulator, ANSYS[‡] High Frequency Structure Simulator (HFSS). This is the case when the data deterioration due to the VNA measurement limit is omitted and simulated S_{11} becomes only small at the resonance. As a test sample for the simulation, a very low-loss non-dispersive magnetic material was considered whose relative permittivity and permeability are $\varepsilon_r = 10.000 - j0.001$ ($\tan \delta_e = 0.0001$) and $\mu_r = 25.0000 - j0.0025$ ($\tan \delta_m = 0.0001$). We placed the test sample into a 7-mm coaxial transmission line (APC-7) known to operate up to 18 GHz with no higher-order modes when loaded with a polytetrafluoroethylene (PTFE) dielectric insulator. We configured the sample length to be $L = 5$ mm so that the $\lambda/2$ resonance occurs below 18 GHz.

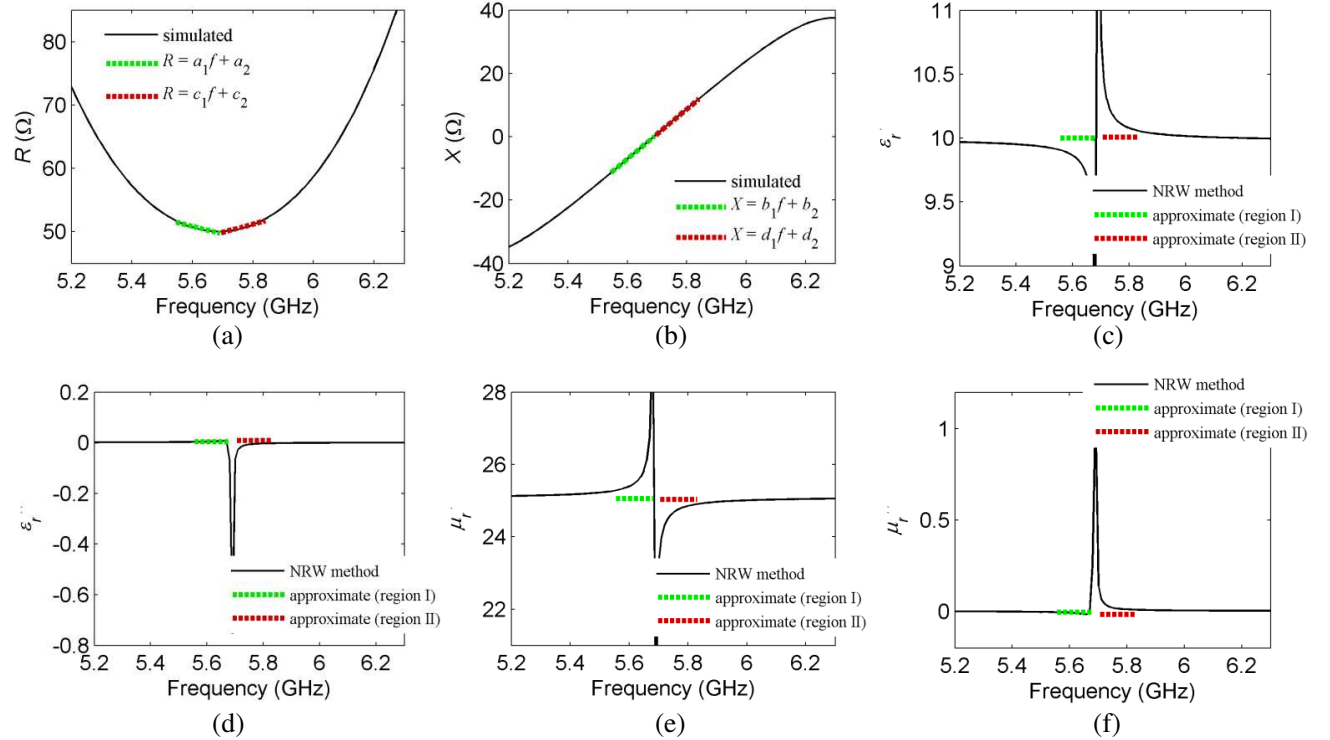


Figure 7. Input impedance, permittivity and permeability extracted from the simulated data for the coaxial transmission line. (a) R , (b) X , (c) ε'_r , (d) ε''_r , (e) μ'_r and (f) μ''_r (green and red dashed lines respectively represent our approximate data in regions I and II).

[‡] Reference to specific software in this article is provided for informational purposes only and constitutes no endorsement by the National Institute of Standards and Technology.

The simulated input impedance Z_{in} of the sample-loaded transmission line is shown in Figs. 7(a) and (b), exhibiting a $\lambda/2$ resonance at $f_0 = 5.69$ GHz, where $R = 50.0500 \Omega$ (minimal) and $X = 0.0975 \Omega$ (close to zero). Selecting $f_A = 5.54$ GHz and $f_B = 5.84$ GHz to apply our approximate approach, we made use of a built-in function of the commercial numerical software package, MATLAB[§], for finding the regressions as plotted in Figs. 7(a) and (b). The resultant regression coefficients are $a_1 = -12.0486$, $b_1 = 78.6471$, $c_1 = 13.0710$, and $d_1 = 78.6003$. By solving Eqs. (21)–(24) with these regression coefficients and the initial values taken from outside the resonance to find the characteristic impedance Z , and then by substituting Z into Eq. (25), we obtained the wave impedance ζ of the test sample. The relative permittivity and permeability in Figs. 7(c)–(f) were calculated from $\epsilon_r = n/\zeta$ and $\mu_r = n \cdot \zeta$ with a knowledge of the refractive index n obtained from Eq. (14) for the NRW algorithm.

Figures 7(c) and (e) show that ϵ'_r and μ'_r from the NRW method have large discrepancies compared to the values configured for the simulation at f_A and f_B , and we can confirm that f_A and f_B we selected are within the frequency band of the half-wavelength resonance. In Figs. 7(c)–(f), ϵ_r and μ_r approximated with our approach seem to be very consistent across regions I and II, and it is validated that our assumption to derive the approximation — material parameters of test samples are constant around the resonance — is adequate. In Figs. 7(c)–(f), the approximate permittivity and permeability are shown to be $\epsilon_r = 9.999 - j0.004$ and $\mu_r = 25.0540 + j0.0050$ in region I, and $\epsilon_r = 10.008 - j0.009$ and $\mu_r = 25.0310 + j0.0170$ in region II, agreeing very well with the values we input in the simulation, whereas the NRW material parameters are shown to be very divergent at the $\lambda/2$ resonant frequency.

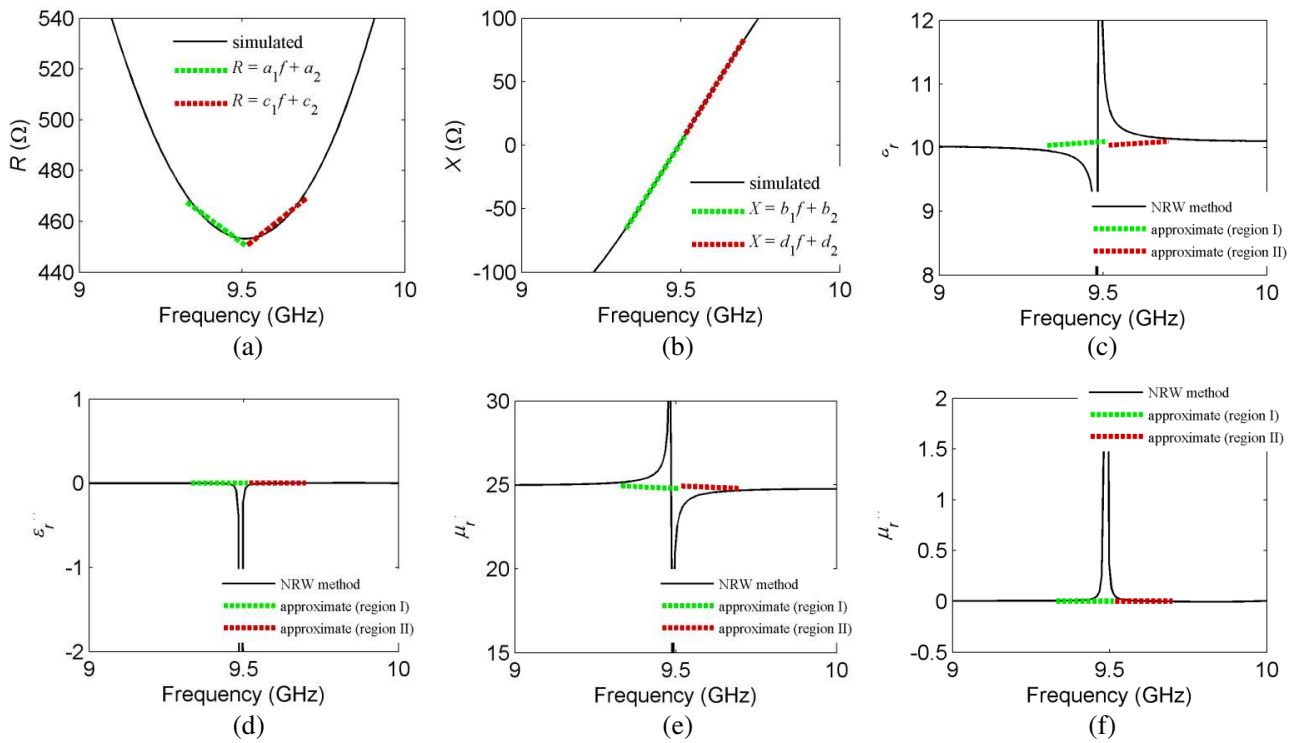


Figure 8. Input impedance, permittivity and permeability extracted from the simulated data for the rectangular waveguide. (a) R , (b) X , (c) ϵ'_r , (d) ϵ''_r , (e) μ'_r and (f) μ''_r (green and red dashed lines respectively represent our approximate data in regions I and II).

Next, we attempted to test out our current approximate approach with S -parameters simulated for the same sample installed in a rectangular waveguide in place of the coaxial transmission line. In the simulation model, we used a WR-112 waveguide whose operational frequency is 7.05–10 GHz (H band).

[§] Reference to specific software in this article is provided for informational purposes only and constitutes no endorsement by the National Institute of Standards and Technology.

The sample length was chosen to be $L = 5$ mm so that the resonance occurs within that frequency range. From the plots for the input impedance in Figs. 8(a) and (b), we see that the resonant frequency is $f_0 = 9.5125$ GHz, where $R = 453.2300 \Omega$ (minimal), which is very close to the characteristic impedance of the air-filled waveguide at f_0 , and $X = 4.3849 \Omega$ (very small). Choosing $f_A = 9.325$ GHz and $f_B = 9.700$ GHz, we obtained $a_1 = -94.8193$, $b_1 = 394.7375$, $c_1 = 101.8847$, and $d_1 = 404.9929$. Using Eqs. (21)–(24), and Eq. (26) with these regression coefficients, we extracted the relative permittivity and permeability, as shown in Figs. 8(c)–(f). In regard to the waveguide measurement, the extracted relative permittivity and permeability seem to have minimal slopes unlike those in the coaxial transmission line measurement. This is attributed to the fact that Eq. (26) for μ_r , calculated from a_1 , b_1 , c_1 , and d_1 for approximating the input impedance Z_{in} (in turn, the characteristic impedance Z), contains n as acquired from the NRW method and not necessarily very constant in the rectangular waveguide measurement. The approximate permittivity and permeability shown in Figs. 8(c)–(f), $\epsilon_r = 10.070 - j0.001$ and $\mu_r = 24.8622 - j0.0025$ at 9.4 GHz in region I and $\epsilon_r = 10.066 - j0.001$ and $\mu_r = 24.8584 - j0.0025$ at 9.6 GHz in region II, exhibit very good agreement with those we used in the simulation. In contrast, the NRW results generate very divergent peaks at the $\lambda/2$ resonance, just as for the coaxial-transmission-line case.

Also, we examined our approach using measured S -parameters shown in Figs. 2(a) and (b) for nylon of $L = 15.1$ mm. Figs. 9(a) and (b) show extracted ϵ'_r and ϵ''_r for nylon by comparison to the results from the BJ iterative method which uses only Eq. (13) for dielectric-only measurements and is considered to be one of the most accurate methods for broadband dielectric measurements, since Eq. (13) is a function of S_{21} and S_{12} , not of S_{11} nor of S_{22} [13, 14]. Uncertainty bounds are given in Figs. 9(a) and (b) with regard to the data obtained from the BJ method. Moderately strict dimensional errors ($+/- 4 \mu\text{m}$) for the sample and fixture were input in order to calculate these uncertainties. Note that because in this case the BJ method can determine only the permittivity, and as well is a reference-plane invariant

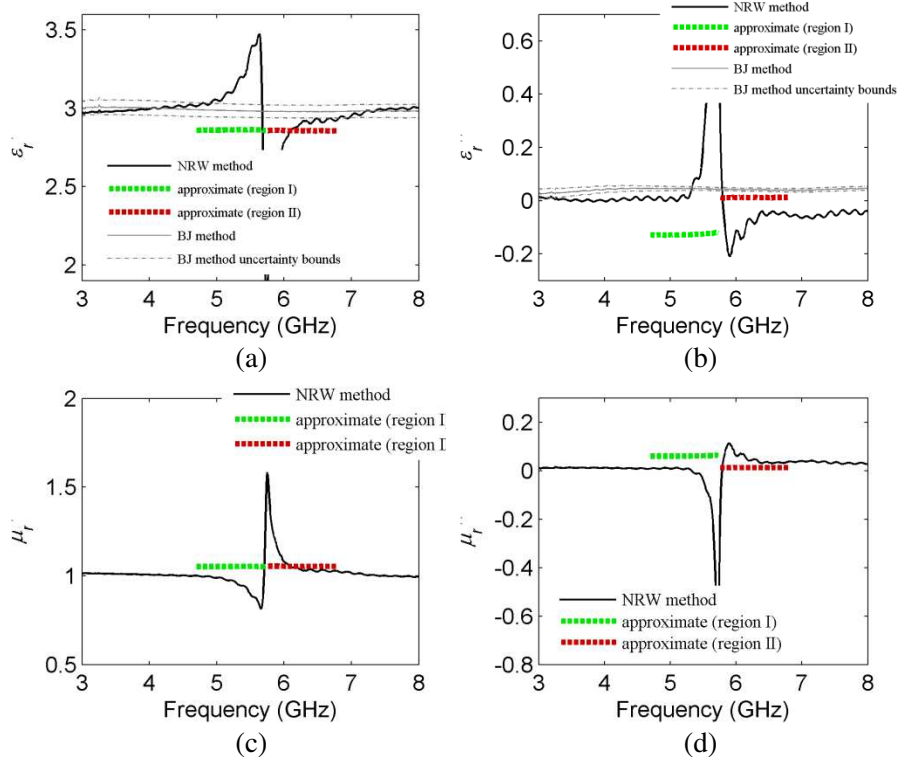


Figure 9. Nylon permittivity and permeability extracted from measured S -parameters. (a) ϵ'_r , (b) ϵ''_r , (c) μ'_r and (d) μ''_r (green and red dashed lines respectively represent our approximate data in regions I and II).

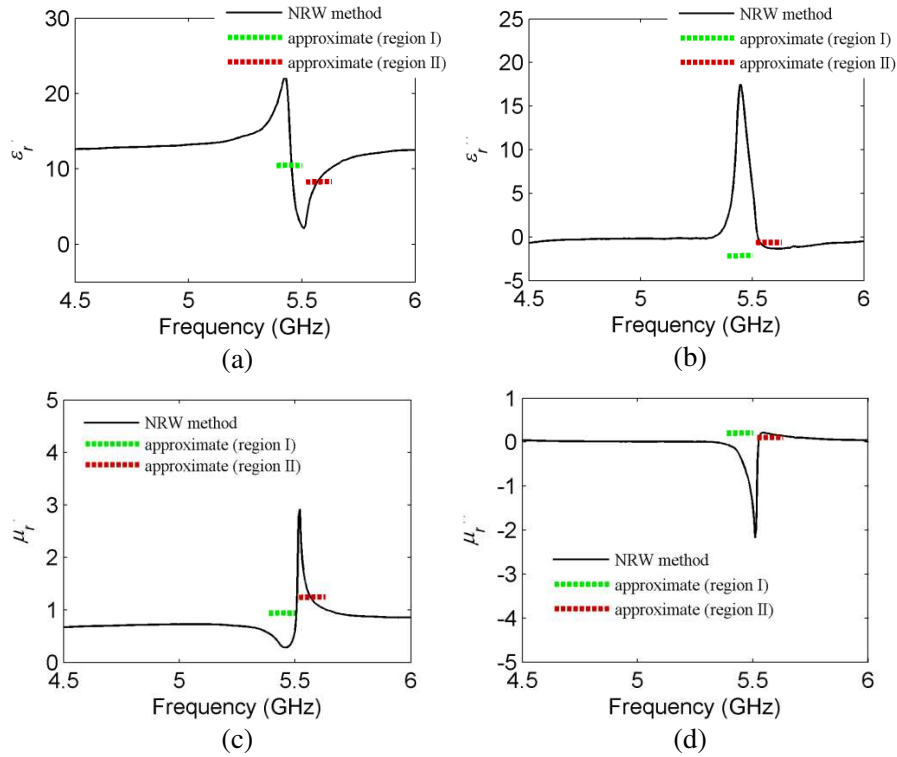


Figure 10. Lithium ferrite permittivity and permeability extracted from measured S -parameters. (a) ε'_r , (b) ε''_r , (c) μ'_r and (d) μ''_r (green and red dashed lines respectively represent the data in regions I and II).

algorithm, the uncertainties that the present approximation and conventional T/R methods may suffer from are greatly eliminated with the BJ method.

In Figs. 9(a) and (b), we see that the approximate method gives $\varepsilon_r = 2.864 + j0.1216$ and $\varepsilon_r = 2.858 - j0.032$, respectively, in regions I and II, showing relatively good agreement with the lower bounds for the BJ data ($\varepsilon_r = 2.940 - j0.038$ and $\varepsilon_r = 2.939 - j0.045$) in regions I and II, whereas the NRW method has a very large divergent spurious peak at the $\lambda/2$ resonance. In Figs. 9(c) and (d), our approximate permeability appears to be $\mu_r = 1.052 - j0.061$ and $\mu_r = 1.053 - j0.014$ in regions I and II, respectively, while the NRW permeability again results in the artifact at the $\lambda/2$ resonance.

For a second experimental test, we measured a sample of a low-loss magnetic material, lithium ferrite, with the APC-7 coaxial transmission line. Figs. 10(a)–(d) show the permittivity and permeability extracted by means of both the NRW and our approximate methods. These plots show that the results from the NRW method include very prominent artifacts, whereas our approximation generates roughly $\varepsilon_r \approx 10$ and $\mu_r \approx 1.1$ near the resonance. We deduce that disagreements between regions I and II originate from lithium ferrite's slightly dispersive properties in these frequency regions.

Both simulation and experimental results in this section confirm that our approximate approach gives considerably more accurate data near the half-wavelength resonance than does the NRW method in both the simulations and experiments (also more accurate than the BJ method for magnetic measurements). We emphasize that the approximate approach proposed in this paper can be applied whether a test material is dielectric or magnetic as long as the material possesses flat material properties at the half-wavelength resonant frequencies. Note that, at this point, we have manually selected f_A and f_B by visual inspection of the resonant frequency bands by checking where the material parameters resulting from the conventional T/R methods start to show oscillation, and thus that the accuracy of our approximate approach presented in this paper may depend on a way of choosing f_A and f_B .

4. CONCLUSION

We have developed an approximate method for measuring permittivities and permeabilities near half-wavelength resonances. The approach approximates the characteristic impedance Z of the sample-filled section of the transmission line with 1st-order regression coefficients for the input impedance Z_{in} of the sample-loaded transmission line at each of two frequency regions I and II around the resonant frequency. Either of ζ of the sample loaded in the coaxial transmission line or μ_r in the rectangular waveguide is calculated from the approximate characteristic impedance Z . The other material parameters are easily obtained by employing n calculated from the conventional T/R method.

We have validated our approximate method with simulated S -parameters for both coaxial transmission line and rectangular waveguide measurements. The results from our method are in very good agreement with the values configured for the simulations. In contrast, the NRW method exhibits strong divergent artifacts at the $\lambda/2$ resonances.

Furthermore, we have extracted nylon permittivity and permeability from experimentally measured S -parameters. Our approximate approach shows smooth ε_r , that is close to the lower bounds of the nylon permittivity estimated by the BJ dielectric-only method, and the permeability $\mu_r \approx 1$, whereas the NRW method leads to a very large spurious peak in both permittivity and permeability at the $\lambda/2$ resonance. We have also measured lithium ferrite and have confirmed that relatively better results are obtained from the approximate approach than those from the NRW method. To reiterate, we emphasize that the NRW and BJ methods generate resonant artifacts when simultaneously extracting permittivities and permeabilities of low-loss materials around $\lambda/2$ resonances. The BJ data shown in Section 3 for comparison are the results from the T method that does not extract μ_r .

At present, we are investigating the reasonable bounds of the material parameters determined from the T/R methods to choose physically justifiable f_A and f_B where the extracted parameters start to deviate from the real ones. That extended study will give us a robust way of choosing f_A and f_B , which will be reported in a future publication.

ACKNOWLEDGMENT

The authors thank Michael D. Janezic, Jack Surek, and Bill Riddle of the National Institute of Standards and Technology (NIST) in Boulder, Colorado, USA, for some helpful discussions.

REFERENCES

1. Chen, L. F., C. K. Ong, C. P. Neo, V. V. Varadan, and V. K. Varadan, *Microwave Electronics: Measurement and Materials Characterization*, Wiley, NJ, 2004.
2. Baker-Jarvis, J., M. D. Janezic, B. F. Riddle, R. T. Johnk, P. Kabos, C. L. Holloway, R. G. Geyer, and C. A. Grosvenor, "Measuring the permittivity and permeability of lossy materials: Solids, liquids, metals, building materials, and negative-index materials," National Institute of Standards and Technology Technical Note 1536, 2003.
3. Baker-Jarvis, J., M. D. Janezic, and D. C. DeGroot, "High-frequency dielectric measurements," *IEEE Instrum. Meas. Magazine*, Vol. 13, 24–31, 2010.
4. Fenner, R. A., E. J. Rothwell, and L. L. Frasch, "A comprehensive analysis of free-space and guided-wave technique for extracting the permittivity and permeability of materials using reflection-only measurements," *Radio Sci.*, Vol. 47, RS1044, 2012.
5. Chalapat, K., K. Sarvala, J. Li, and G. S. Paraoanu, "Wideband reference-plane invariant method for measuring electromagnetic parameters of materials," *IEEE Trans. Microw. Theory Tech.*, Vol. 57, 2257–2267, 2009.
6. Qi, J., H. Kettunen, H. Wallen, and A. Sihvola, "Compensation of Fabry-Perot resonances in homogenization of dielectric composites," *IEEE Antennas Wireless Propag. Lett.*, Vol. 9, 1057–1060, 2010.
7. Liu, X.-X., D. A. Powell, and A. Alu, "Correcting the Fabry-Perot artifacts in metamaterial retrieval procedures," *Phys. Rev. B*, Vol. 84, 235106, 2011.

8. Boughriet, A.-H., C. Legrand, and A. Chapoton, "Noniterative stable transmission/reflection method for low-loss material complex permittivity determination," *IEEE Trans. Microw. Theory Tech.*, Vol. 45, 52–57, 1997.
9. Hasar, U. C., "Two novel amplitude-only methods for complex permittivity determination of medium- and low-loss materials," *Meas. Sci. Technol.*, Vol. 19, 055706, 2008.
10. Hasar, U. C. and C. R. Westgate, "A broadband and stable method for unique complex permittivity determination of low-loss materials," *IEEE Trans. Microw. Theory Tech.*, Vol. 57, 471–477, 2009.
11. Nicolson, A. M. and G. F. Ross, "Measurement of intrinsic properties of materials by time-domain techniques," *IEEE Trans. Instrum. Meas.*, Vol. 19, 377–382, 1970.
12. Weir, W. B., "Automatic measurement of complex dielectric constant and permeability at microwave frequencies," *Proc. IEEE*, Vol. 62, 33–36, 1974.
13. Baker-Jarvis, J., E. J. Vanzura, and W. A. Kissick, "Improved technique for determining complex permittivity with transmission/reflection method," *IEEE Trans. Microw. Theory Tech.*, Vol. 38, 1096–1103, 1990.
14. Baker-Jarvis, J., M. D. Janezic, J. H. Grosvenor, Jr., and R. G. Geyer, "Transmission/reflection and short-circuit line method for measuring permittivity and permeability," National Institute of Standards and Technology Technical Note 1355-R, 1993.
15. Smith, D. R. and S. Schultz, "Determination of effective permittivity and permeability of metamaterials from reflection and transmission coefficients," *Phys. Rev. B*, Vol. 65, 195104, 2002.
16. Chen, X., T. M. Grzegorzczuk, B.-I. Wu, J. Pachenco, Jr., and J. A. Kong, "Robust method to retrieve the constitutive effective parameters of metamaterials," *Phys. Rev. E*, Vol. 70, 1–7, 2004.
17. Barroso, J. J. and A. L. de Paula, "Retrieval of permittivity and permeability of homogeneous materials from scattering parameters," *Journal of Electromagnetic Waves and Applications*, Vol. 24, Nos. 11–12, 1563–1574, 2010.
18. Pozar, D. M., *Microwave Engineering*, 2nd Edition, Ch. 6, Wiley, NJ, 1998.
19. Challa, R. K., D. Kajfez, J. R. Gladden, and A. Z. Elsherbeni, "Permittivity measurement with non-standard waveguide by using TRL calibration and fractional linear data fitting," *Progress In Electromagnetics Research B*, Vol. 2, 1–13, 2010.